Stats:

Word count: 4642, from Introduction to end of References, including figure captions.

Abstract length: 246 words

SHORT COMMUNICATION

Both near-surface and satellite remote sensing confirm drought legacy effect on tropical forest leaf phenology after 2015/2016 ENSO drought

Nathan Borges Gonçalves [1,2], Aline Pontes Lopes [3], Ricardo Dalagnol [3], Jin Wu[4], Davieliton Mesquita Pinho[1] Bruce Walker Nelson[1]

[1] INPA – National Institute for Amazon Research, Environmental Dynamics Department, Manaus, AM, {nathanborges, bnelsonbr, davieliton.ufpa}@gmail.com

[2] Michigan State University, Department of Forestry, College of Agriculture & Natural Resources, East Lansing, MI, USA, nathanborges@gmail.com;

[3]INPE – National Institute for Space Research, Remote Sensing Division, São José dos Campos, SP, alineplopes@gmail.com; ricds@hotmail.com;

[4] University of Hong Kong, School of Biological Sciences, jinwu@hku.hk.

Corresponding author: Nathan Borges Gonçalves (nathanborges@gmail.com)

Abstract

Amazon forest leaf phenology patterns have often been inferred from the Moderate Resolution Imaging Spectroradiometer (MODIS) Enhanced Vegetation Index (EVI). But reliable MODIS detection of seasonal and interannual leaf phenology patterns has also been questioned and is generally not validated with field observation. Here we compare inter-annual patterns of local-scale upper canopy leaf phenology and demography derived from tower-mounted phenocams at two upland forest sites in the Central Amazon, to corresponding satellite vegetation indices retrieved from MODIS-MAIAC (Multi-Angle Implementation of Atmospheric Correction). We focus on forest response to an unprecedented drought caused by the El Niño of 2015-16. At both sites, multi-year phenocam data showed post-drought shifts in leaf demography. These were consistent with MODIS-MAIAC anomalies in two vegetation indices. Specifically, a precocious leaf flush at both sites during the first two post-drought months, Feb-Mar 2016, caused (1) an anomalous decrease in flushing trees in Jun-Jul of 2016 and (2) an increase of trees with early mature stage leaves (2-4 mo age) in Apr-May-Jun of 2016. At both sites, these two phenological anomalies showed up in MODIS-MAIAC as, respectively, (1) a strong negative anomaly in Gcc (Green chromatic coordinate), which prior work has shown to be sensitive to the abundance of leaves 0-1 mo old, and (2) a strong positive anomaly in EVI, which is sensitive to abundance of leaves 2-4 mo age. A shift to sub-optimal seasonal leaf age mix is expected to change the ecosystem-scale intrinsic photosynthetic capacity for ~18 month after the drought.

Keywords: MODIS-MAIAC, Amazon green-up, EVI seasonality, phenocam, leaf demography, El Niño

1. Introduction

Conflicting patterns have been reported for drought effect on both seasonal and interannual green-up in Amazon forests. For the 2005 drought, Saleska et al. (2007) found an anomalously high dry-season MODIS EVI. Detectability of this anomaly was contested by Samanta et al. (2011) due to poor cloud and aerosol screening in MODIS collection 5. Furthermore, during or shortly after the drought in 2005 tree mortality increased, and more so where drought was most intense (Phillips et al., 2009). A dry-season brown-down was reported across Amazonia during a 2010 drought (Xu et al., 2011; Hilker et al., 2014).

Increasing EVI as a typical Central Amazon dry season progresses was first reported by Huete et al. (2006). This was later shown to be due in part to sun-sensor geometry artifacts (Morton et al., 2014). Solar zenith angle decreases over most of the Amazon during the drier months, reducing sub-pixel shadow fraction and thus increasing near-infrared reflectance and EVI (Galvão et al., 2011).

MODIS-MAIAC (Multi-Angle Implementation of Atmospheric Correction), developed by Lyapustin et al. (2012), offered hope for settling the debate over MODIS detectability of leaf phenology in the Amazon by providing improvements in cloud and aerosol filtering and in the correction of sun-sensor geometry artifacts. Four recent studies of Central Amazon upland forests combined monthly MODIS-MAIAC with leaf demography data obtained from tower-mounted RGB cameras (phenocams), and with other data, to ask if MODIS-MAIAC seasonal patterns are consistent with the large seasonal change in leaf demography observed with the phenocams. The complimentary data evaluated in each study were: (1) tree crown phenostages from a high resolution orbital sensor (Lopes et al., 2016); (2) Gross Ecosystem Productivity and leaf-level photosynthetic efficiency as a function of leaf age (Wu et al., 2016); (3) leaf spectra by age class and age

class abundance, driving a radiative transfer model (Wu et al., 2018); and (4) Landsat 8 images with constant sun-sensor geometry compared across different seasons (Gonçalves et al., 2019). All four studies found that during normal climate years there are large seasonal changes in leaf demography in the Central Amazon (Figure S1, Video S1) and these are detected by MODIS-MAIAC.

Here we ask if (1) more subtle interannual changes in leaf phenology occurred during or after the 2015-16 El Niño and, if so, (2) whether these anomalies were detected by MODIS-MAIAC. To this end, we examine long (> 5 year) records of leaf flush by crown and the derived leaf demography for the upper forest canopy using phenocams. We then compare the drought-associated deviations in phenocam-based leaf demography to monthly anomalies in two vegetation indices derived from MODIS-MAIAC.

2. Methods

2.1. Climate variables

For a local characterization of the intensity of the 2015-16 El Niño at our Central Amazon phenocam sites, we report anomalies for three climate variables relevant to leaf phenology. These are drought intensity, maximum daily air temperature and solar irradiance at the forest canopy surface. These require long and gap-free records, so we used data from orbital sensors and reanalysis. We obtained monthly rainfall for 21 years (1998-2018) from the Tropical Rainfall Measuring Mission (TRMM 3B43 version 7). As a measure of drought intensity, we extracted the Maximum Cumulative Water Deficit (MCWD) for each string of consecutive dry months (< 100 mm mo^{-1}), as per Malhi et al. (2009). We obtained daily maximum near surface (2 meters) air temperatures from the MERRA-2 Reanalysis for the 39y period 1980 to 2018. We used the CERES EBAF Edition 4.0 surface data product

(Kato et al., 2018) to retrieve monthly means, from March 2000 to March 2018, of surface downwelling shortwave radiant flux under all-sky conditions. CERES EBAF shortwave irradiance was well correlated with above-canopy field measurements (r = 0.93 for year 2015) and is an excellent proxy for downwelling Photosynthetically Active Radiation (r = 0.99; Papaioannou et al., 1993).

2.2. Leaf demography from phenocams

We monitored upper canopy leaf phenology daily for 64 months and 72 months, respectively, at the ATTO and k34 tower sites in the Central Amazon region of Brazil. ATTO is at 2° 8'36"S, 59° 0’2"W, 150 km northeast of Manaus, while k34 is at 2°36'33"S, 60°12'33"W, 60 km northwest of Manaus. The towers are 145 km apart and have similar climate and forests on well-drained oxisol plateaus. At both sites we employed the RGB Stardot Netcam model XL 3MP. The ATTO phenocam with 96^{o} HFOV lens was mounted ~50 m above the forest canopy surface and tracked 195 upper canopy tree crowns spread over four hectares. At k34 we tracked 42 crowns with a 66^{o} HFOV lens from 15m above the canopy, covering about one hectare. Both cameras were set to an interpolated resolution of 2048 x 1536 pixels with automatic color balance turned off and auto-exposure turned on.

The age of each crown’s leaf cohort was determined by visually detecting the date of the entire crown’s abrupt leaf flush, which occurs in most Central Amazon trees once per year. Visual detection of flush in each crown is reliable (see Video S1, animated gif in Supplementary Data 2). Leaf flush can also be detected digitally as a spike in the Green chromatic coordinate (Gcc) of each crown timeline, with an accuracy of 83% when compared to visual detection (Lopes et al., 2016). Gcc is the fractional contribution of the

visible green band brightness to the sum of red, green and blue bands (Woebbecke et al., 1995).

Though not essential for visual flush detection, we controlled for artifacts associated with different linear responses of the three RGB channels by selecting images with similar exposure times. Shifting shadows from changing solar elevation and azimuth were eliminated by using only diffusely lit images, taken under overcast sky. The images were captured from mid-morning to early afternoon at two minute intervals, a frequency that improves chances of obtaining daily diffuse-lit images. Flush detections in daily images were aggregated to obtain a monthly census of leaf flush events by crown, from which we derived the monthly leaf age mix (leaf demography) for the full set of upper canopy crowns within the phenocam view. Following Lopes et al. (2016), we assumed complete upper crown leaf turnover during the month of leaf flush and a mean leaf residence time of 12 months. The latter is consistent with leaf area turnover time of 12.4 months (Valle, 2016), derived from monitoring canopy leaf area stock and leaf area in litterfall at monthly intervals.

2.3. MODIS-MAIAC vegetation indices

Two vegetation indices, EVI and Gcc, were calculated for the period 2001-2016 from MODIS-MAIAC surface reflectance bands corrected to an apparent view zenith angle of 0^o and an apparent solar zenith angle of 45^o, following Lyapustin and Wang (2018). Temporal resolution was 16 days and spatial resolution was 1 km. The correction is an empirical inversion that requires several cloud-free measurements of the same pixel in each 16-day period, during which the sun-sensor geometry of that pixel varies (Lyapustin et al., 2012; Moura et al., 2012). Within each 16-day period, canopy spectral pattern is assumed to

be constant and all differences are attributed to the view and illumination geometry effects which are being removed.

MAIAC EVI was calculated using the equation in Huete et al. (2002). MAIAC Gcc was calculated as for phenocams, using surface reflectance of red, green and blue bands. We used the spatial average of each index within a window of 8x11 MODIS-MAIAC pixels centered on each of the two phenocam-equipped micromet towers and covering only plateau areas. This window size was chosen to balance the noise reduction benefit of a large window against the need to avoid water bodies and minimize the inclusion of broad areas with poorly drained forests. In addition to the oxisol plateau forest monitored by the phenocams, other forested habitats occupy both 88-km^2 areas of interest, such as well drained oxisol on upper slopes and poorly drained podzol on lower slopes and stream margins. But these forests are all very similar to the phenocam's plateau forests in their seasonality of LAI, leaf drop, leaf flush and leaf residence times, based on monitoring of monthly leaf litterfall and LAI (Valle, 2016).

Standardized anomalies of the two vegetation indices were obtained for each month of the MAIAC window time series using the statistical and computational platform R (R Development Core Team, 2017) and the raster package (Hijmans & van Etten, 2016). We also investigated standardized anomalies per trimester and bimester. We explored how anomalies during and after the 2015-16 ENSO in the Central Amazon might be linked to leaf demography changes at the two tower sites. Standardized anomalies for a vegetation index (VI) were calculated as:

$$Anomaly_{my} = (VI_{my} - Mean(VI_m)) / (SD(VI_m))$$

where VI_my is the observed value for month m of year y, Mean(VI_m) is the 16y mean for month m over the period 2001-2016 and SD(VI_m) is the standard deviation of

161 month m for the same 16y period. Some uncertanties with MODIS-MAIAC product may
162 persist, such as: (1) MAIAC BRDF correction products being less constrained if the
163 inversion model uses fewer observations during cloudy periods; (2) poor cloud screening
164 during cloudy periods and (3) sub-pixel topography effects. Thus, we considered a
165 "significant" anomaly to be at least two standard deviations above or below the 16y mean
166 of a given studied interval.
167
168 ***2.4. Leaf demography and vegetation indices under normal seasonal climate***
169 MODIS-MAIAC Gcc and EVI are well correlated with the frequencies of crowns
170 having, respectively, leaves of 0-1 mo age post-flush and leaves of 2-5 mo age post-flush
171 (Figure S2; see also Gonçalves et al., 2019). This is consistent with other reports of change
172 in leaf-level near-infrared (NIR) reflectance: NIR increases from 0-2 mo and remains high
173 until about seven months of age (Roberts et al., 1998; Yang et al., 2014; Chavana-Bryant et
174 al., 2016; Moura et al., 2017; Wu et al., 2018). Thus, MODIS-MAIAC Gcc is sensitive to
175 the abundance of young leaves and recently flushed crowns, while EVI is sensitive to the
176 abundance of crowns with high-NIR mature leaves.
177
178 **3. Results**
179 ***3.1. Climate panorama in 2015/16***
180 Both Central Amazon tower sites typically have 2-3 dry months per year, i.e., below
181 100 mm mo^{-1}, which is the mean evapotranspiration demand of Amazon rainforests
182 (Aragão et al., 2007, Malhi et al., 2009). But in the seven months beginning in July 2015
183 and ending in January of 2016, rainfall remained below or only slightly exceeded this
184 threshold. The accumulated water deficit relative to demand for these seven months was -

182 mm at k34 tower and -267 mm at ATTO tower. At both sites, the 2015/16 drought reached a record negative MCWD for the 21-year period of TRMM data (Fig. 1B). The drought ended in February 2016 at both sites; monthly rainfalls for February, March, and April of 2016 all exceeded 200 mm mo^{-1} at k34 and 300 mm mo^{-1} at ATTO (Fig.1A).

Monthly means of daily maximum near-surface air temperature reached record highs in the fourth trimester of 2015 (Oct-Nov-Dec): a 2.5 SD positive anomaly at ATTO site and 3.3 SD positive anomaly at k34 (Fig. 1C). Monthly means of the daily near-surface temperature maxima remained above 1 SD positive for the seven consecutive months of drought at both sites. Maximum daily air temperature exceeded 39 ^{o}C during 29 days in 2015 at ATTO and 39 days at k34. The prior annual records since 1980 for this threshold at the two sites were much fewer, 5 and 14 days, respectively.

Downwelling surface shortwave radiation during peak drought did not show large positive anomalies that might have been expected from the unprecedented high air temperatures. For the fourth trimester of 2015, downwelling radiance anomalies were only + 1.49 SD at ATTO (Fig. 1C) and + 1.69 SD at k34 (not shown). The anomaly exceeded + 1 SD in only three non-consecutive months during the ENSO at both sites (Fig.1D).

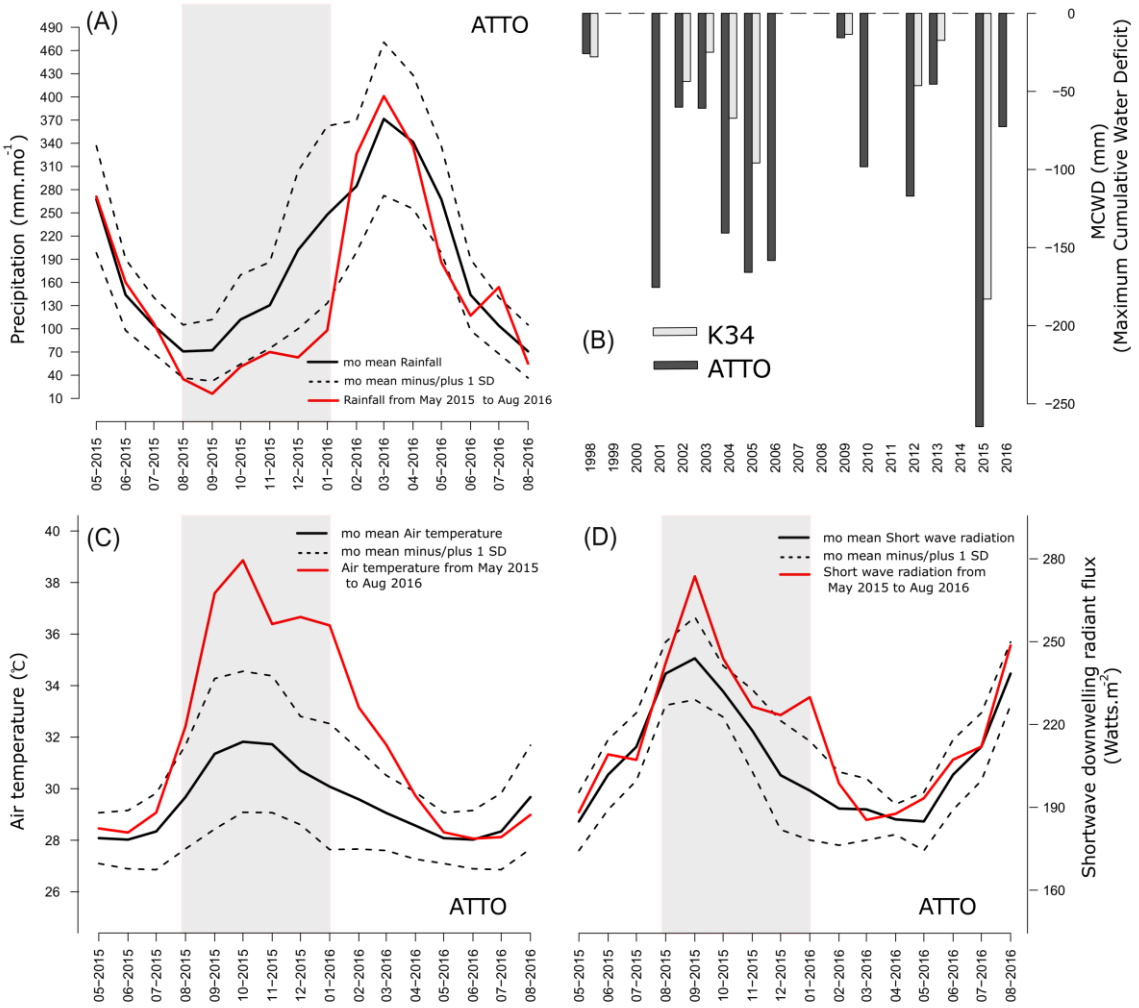

Fig 1. A) Long term monthly mean precipitation (black line) and monthly precipitation from May 2015 to Aug 2016 (red line) at ATTO tower site; B) Maximum cumulative water deficit (MCWD) shown for all sets of consecutive dry months from 1998 to 2016 at k34 and ATTO towers; C) Long term monthly means (black line) of daily maximum near-surface air temperature (^{o}C) and monthly values from May 2015 to Aug 2016 (red line) at ATTO tower; D) Long term monthly means (black line) and monthly values from May 2015 to Aug 2016 (red line) at ATTO, of surface shortwave downwelling radiant flux (watts m^{-2}), based on 24h mean flux under all-sky conditions. Long-term ± 1 SD envelopes are shown as black dashed lines in panels A, C & D. Grey shading indicates six consecutive months during the 2015/16 ENSO with precipitation below -1 SD (and below 100 mm mo^{-1}) at ATTO. Sources are TRMM 3B43v7, 1998-2018, for Panels A & B; MERRA-2 Reanalysis, 1980-2018, for panel C; CERES-EBAF Edition 4, 2000-2018, for panel D.

3.2. Leaf flush response to drought

Figure 2 shows in grey the monthly fractions of all trees that flush new leaves each month at ATTO, as a long-term mean ± 1 SD, from July 2013 to October 2018. The post-El Niño year of 2016 was excluded from the mean and is shown as a black trace. A total of 195 upper canopy tree crowns free of vines were monitored, of which 60-70% underwent massive leaf flush at some month during each year. In normal climate years, about 10% did so in the six wettest months while the other 50-60% flushed in the six drier months of the year. A similar seasonal pattern was seen at k34.

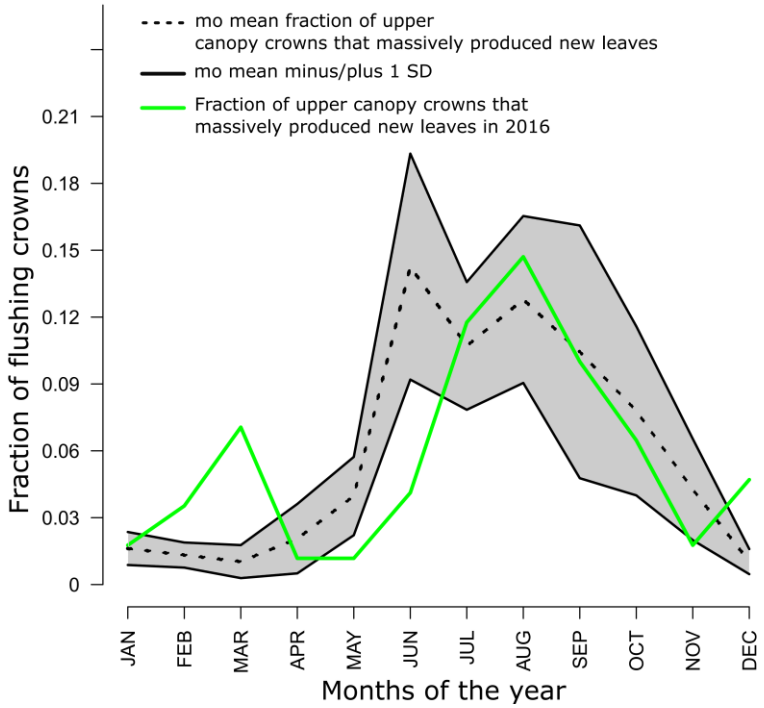

Fig 2. Post El Niño year 2016 (green) and the long-term monthly means ± 1SD for the fraction of all upper canopy crowns that massively produced new leaves at ATTO tower.

Phenocams detected an anomalous and precocious leaf flush in Feb-Mar of 2016 at both sites, immediately after the drought ended. Having already flushed new leaves, these trees forced a paucity of flushing crowns in Jun-Jul of 2016 compared with this same

period in prior non-drought years (Fig. 2, green line; Fig. 3A & B, green lines). The missing flush in Jun-Jul of 2016 at both tower sites was detected as large negative anomalies (< -2 SD) in MODIS-MAIAC Gcc for Jun-Jul of 2016 (black bars in Fig 3 A, B).

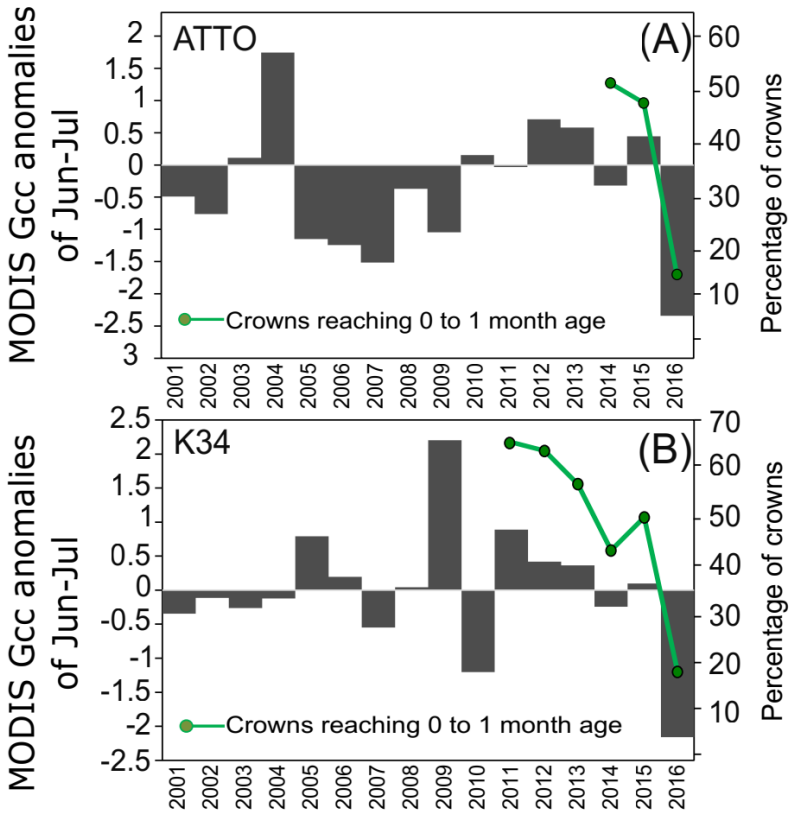

Fig. 3. (A) Standardized anomalies of MODIS-MAIAC Gcc for the 16 annual periods of Jun-Jul at ATTO tower (black bars) plotted against the percentage of recently flushed crowns in this same two-month period (green trace); Jun-Jul is when massively flushing crowns reach their annual peak under normal climate (see Fig. 2); (B) same as A, but for k34 tower. The "percentage of crowns" that recently flushed is with respect to the total number of crowns that flushed in a year; non-flushing crowns are excluded from the calculation.

Maturing leaves from the precocious flush in Feb-Mar of 2016 led to anomalously high fractions of crowns with early-mature stage leaves (green traces in Fig. 4). These were associated at both sites with a large positive anomaly (>2.5 SD) for MODIS-MAIAC EVI in the second trimester of 2016 (Apr-May-Jun) (black bars in Fig. 4 A&B).

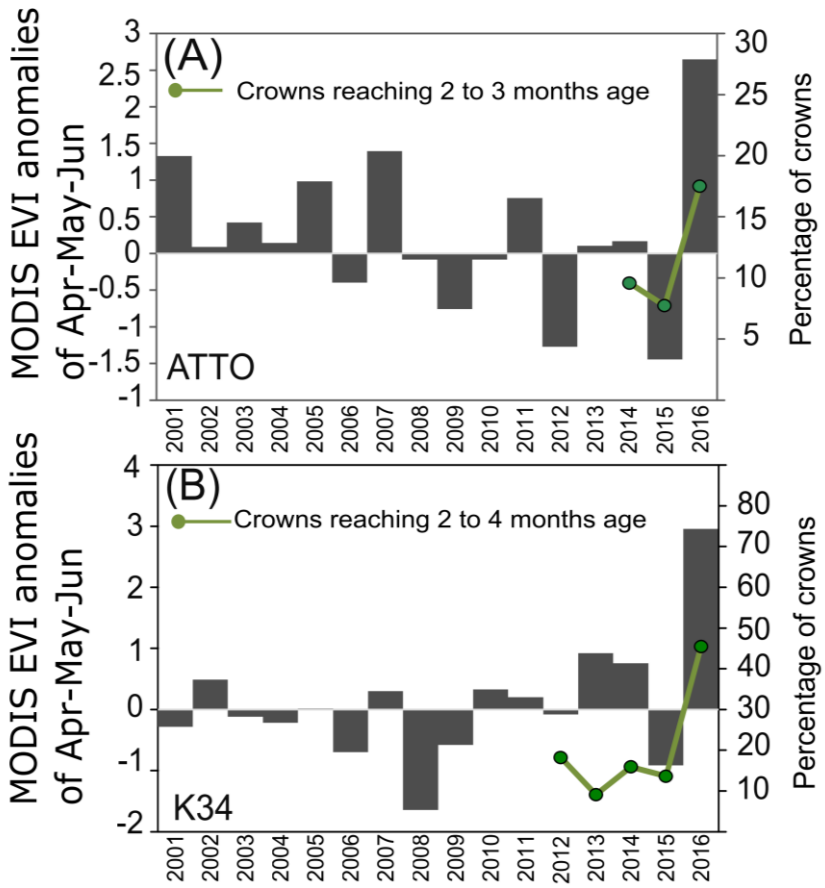

Fig 4. A) Anomalies of MODIS-MAIAC EVI at the ATTO site for the second trimester of each year (Apr-May-Jun) and the percentage of crowns with massively flushed leaves reaching early mature stage (2-3 months age at ATTO and 2-4 months age at K34), also in the second trimester of each year. The "percentage of crowns" is with respect to the total number of crowns that flushed in a year; non-flushing crowns are excluded from the calculation.

4. Discussion and Conclusions

Our two questions are answered in the following affirmative. First, phenocams at two Central Amazon towers detected shifts in forest leaf phenology after the seven-month long drought of the 2015-16 El Niño. Anomalies in leaf flush frequency were seen up to six months after the start of post-drought rains. Second, these anomalies were detected by MODIS-MAIAC. Given the upper canopy leaf lifespan, this drought-legacy remained in

257 place as a possibly sub-optimal leaf age mix in the upper canopy for ~18 months after the
258 drought ended.

259 Reliable detection by orbital sensors of the spectral changes associated with the
260 abundance of different leaf age classes is important because leaf demography controls
261 seasonality of photosynthetic efficiency in Amazon forests (Wu et al., 2016). Two
262 important prior critiques of the reliability of MODIS collection 5 detection of Central
263 Amazon seasonal spectral change were (1) seasonal artifacts from cloud contamination
264 (Samanta et al., 2011) and (2) the decrease in solar zenith angle during the dry season, from
265 June to October, leading to decreasing sub-pixel shade fraction and concomitant artefactual
266 increase in NIR reflectance (Galvão et al., 2012; Morton et al., 2014). Our results show
267 that MODIS-MAIAC Gcc and EVI vegetation indices detected not only the large seasonal
268 change in the fractions of leaves in the young and mature age classes during years of
269 normal climate (Gonçalves et al., 2019), but also smaller anomalous shifts in this
270 seasonality associated with the El Niño of 2015/16.

271 Deciphering how different trees' functional traits may be associated with different
272 leaf demography strategies and with the deviations from these strategies after drought, is
273 clearly a next step for study. This may clarify what are the evolutionary pressures that have
274 selected for the most common leaf phenology pattern, which is to produce new leaves in the
275 drier half of the year. Apparent environmental drivers such as total PAR radiant intensity
276 and rainfall (Wagner et al., 2017) may also be (or merely be) cues used by trees to
277 recognize the timing of other selective pressures. Candidates for these underlying drivers
278 include (1) diffuse PAR, which is used more efficiently by the canopy (Gu et al., 2002;
279 Rap et al., 2015; Strada & Unger, 2016; Malavelle et al., 2019) and may be best exploited
280 if its seasonal peak coincides with the photosynthetically efficient mature leaf abundance

and (2) temporal escape from leaf herbivores or leaf pathogens which prefer young leaves (Murali & Sukumar, 1993; Coley & Barrone, 1996), but are inhibited in the dry months.

Interestingly, our data show that the few trees which flush out new leaves in the wet season do not do so consistently. In other years, these same trees flush in the dry season. Wet season flushing may therefore be associated with recovery from stress or disease. The 10% of all trees that participated in the anomalous post-drought flush in Feb-Mar of 2016 were no exception: these trees typically flush in the dry months. A similar pattern was seen in drier forests influenced by monsoon rains in Asia where a second minor leaf flush was detected after a normal drought (Elliot et al., 2006). This suggests that, for the subset of trees showing post-drought flush at our sites, leaves had been physiologically damaged by high temperature and/or drought (Fig. 1; Jimenez et al., 2016; Fontes et al., 2018, Santos et al., 2018) and these leaves were replaced in Feb-Mar, 2016, when the drought ended. Field data on leaf physiology and experiments with artificially forced flushing in different seasons coupled with leaf herbivore census and herbivore exclusion/non-exclusion treatments may help to resolve the underlying selective pressures behind leaf demography strategies in tropical forests.

5. Acknowledgements. We thank the Max Planck Society; the German Federal Ministry of Education and Research; the Brazilian Ministry of Science, Technology, Innovation and Communications (MCTIC); the Amazonas State Foundation for Research (FAPEAM); the Large-scale Biosphere-Atmosphere Experiment of Brazil's National Institute for Amazon Research (LBA/INPA); The Uatumã Sustainable Development Reserve of Amazonas State's Secretariat of Sustainable Development (SDS/CEUC/RDS-Uatumã); FAPEAM financed the GoAmazon project “Understanding the Response of Photosynthetic

Metabolism in Tropical Forests to Seasonal Climate Variations"; The São Paulo Research Foundation (FAPESP), Brazil, grant 2015/22987-7; and the Coordination for the Improvement of Higher Education Personnel (CAPES) provided a two year fellowship for the lead author.

6. Supplementary Data. <Supp_Data1_Goncalves.docx> contains Figures S1 and S2; <Supp_Data2_Goncalves.pptx> contains animated gifs showing two flush events. Video S1 is a one-year time-lapse of the k34 phenocam view showing all flush events by month, available at: <https://drive.google.com/open?id=1VPkCtJKXSSVqnxxVSOfnrQkihGgiwOrY>

7. References

Aragao, L. E. O., Malhi, Y., Roman- Cuesta, R. M., Saatchi, S., Anderson, L. O., & Shimabukuro, Y. E. (2007). Spatial patterns and fire response of recent Amazonian droughts. Geophysical *Research Letters*, 34(7), 1–5.

Chavana- Bryant, C., Malhi, Y., Wu, J., Asner, G. P., Anastasiou, A., Enquist, B. J., ... & Martin, R. E. (2017). Leaf aging of Amazonian canopy trees as revealed by spectral and physiochemical measurements. *New Phytologist*, 214(3), 1049–1063. https://dx.doi.org/10.1111/nph.13853.

Coley, P. D., & Barone, J. A. (1996). Herbivory and plant defenses in tropical forests. *Annual Review of Ecology and Systematics*, 27, 305–335.

Elliott, S., Baker, P. J., & Borchert, R. (2006). Leaf flushing during the dry season: the paradox of Asian monsoon forests. *Global Ecology and Biogeography*, 15(3), 248-257. https://doi.org/10.1111/j.1466-8238.2006.00213.x

329 Fontes, C. G., Dawson, T. E., Jardine, K., McDowell, N., Gimenez, B. O., Anderegg, L., ...
330 & Chambers, J.O. (2018). Dry and hot: the hydraulic consequences of a climate
331 change – type drought for Amazonian trees. *Phil. Trans. R. Soc. B.*, 373 (1760),
332 20180209. http://dx.doi.org/10.1098/rstb.2018.0209
333 Galvão, L.S., Santos, J.R., Roberts, D.A., Breunig, F.M., Toomey, M., Moura, Y.M.
334 (2011). On intra-annual EVI variability in the dry season of tropical forest: A case
335 study with MODIS and hyperspectral data. *Remote Sensing of Environment*, 115,
336 2350–2359. https://doi.org/10.1016/j.rse.2011.04.035
337 Gonçalves, N.B., Lopes.A.P., da Silva, R.D., Wu, J. Nelson, B. W.(2019). Confirming dry-
338 season green-up in Central Amazon forests with Landsat 8 and the role of leaf
339 demography in MODIS-Maiac seasonal spectral patterns. *Proceedings, Brazilian*
340 *Remote Sensing Symposium*, INPE, São Paulo (4 pp).
341 Gu, L., Baldocchi, D., Verma, S.B., Black, T.A., Vesala, T., Falge, E.M., Dowty, P.R.
342 (2002). Advantages of diffuse radiation for terrestrial ecosystem productivity.
343 *Journal of Geophysical Research: Atmospheres* 107(D6):4050.
344 https://doi.org/10.1029/2001JD001242
345 Hijmans, R. J. & van Etten, J. (2012). Raster: geographic analysis and modeling with
346 raster data. R package version 2.0-12. http://CRAN.R-project.org/package=raster
347 Hilker, T., Lyapustin, A. I., Tucker, C. J., Hall, F. G., Myneni, R. B., Wang, Y., ... &
348 Sellers, P. J. (2014). Vegetation dynamics and rainfall sensitivity of the Amazon.
349 *Proceedings of the National Academy of Sciences*, 111(45), 16041–16046.
350 https://doi.org/10.1073/pnas.1404870111.

351 Huete, A., Didan, K., Miura, T., Rodriguez, E. P., Gao, X. & Ferreira, L. G. (2002).
352 Overview of the radiometric and biophysical performance of the MODIS vegetation
353 indices. *Remote Sensing of Environment* 83(1-2), 195–213.
354 Huete, A. R., Didan, K., Shimabukuro, Y. E., Ratana, P., Saleska, S. R.,Hutyra, L. R., &
355 Myneni, R. B. (2006). Amazon rainforests green-up with sunlight in dry season.
356 *Geophysical Research Letters*, 33(6), L06405.
357 https://dx.doi.org/10.1029/2005GL025583
358 Jimenez, J.C., Mattar, C., Barichivich, J., Santamaría-Artigas, A., Takahashi, K., Malhi, Y.,
359 ... van der Schrier, G. (2016). Record-breaking warming and extreme drought in the
360 Amazon rainforest during the course of El Niño 2015–2016. *Scientific Reports*, 6,
361 33130. https://doi.org/10.1038/srep33130.
362 Kato, S., Rose, F.G., Rutan, D.A., Thorsen, T.J., Loeb, N.G., Doelling, D.R., ... & Ham,
363 S.H. (2018). Surface irradiances of edition 4.0 clouds and the Earth's radiant energy
364 system (CERES) energy balanced and filled (EBAF) data product. *Journal of*
365 *Climate*, 31(11), 4501–4527. https://doi.org/10.1175/JCLI-D-17-0523.
366 Lopes, A. P., Nelson, B.W., Wu, J., Graça, P. M. L.,Tavares, J. V., Prohaska, N., ...
367 Saleska,S.R.(2016). Leaf flush drives dry season green-up of the Central Amazon.
368 *Remote Sensing of Environment*, 182: 90–98.
369 https://doi.org/10.1016/j.rse.2016.05.009.
370 Lyapustin, A. I.,Wang, Y., Laszlo, I., Hilker, T. G., Hall, F., Sellers, P. J., & Korkin, S. V.
371 (2012). Multiangle implementation of atmospheric correction for MODIS
372 (MAIAC): Atmospheric correction. *Remote Sensing of Environment*, 127, 385–393.
373 https://dx.doi.org/10.1016/j.rse.2012.09.002.

374 Lyapustin, A.; Wang, Y. (2018). MODIS Multi-Angle Implementation of Atmospheric
375 Correction (MAIAC) *Data User's Guide v. 2.0*. http://modis-
376 land.gsfc.nasa.gov/pdf/MCD19_UserGuide_final_Feb-6-2018.pdf
377 Malavelle, F.F., Haywood, J.M., Mercado, L.M., Folberth, G.A., Bellouin, N. Sitch, S.,
378 Artaxo, P. (2019). Studying the impact of biomass burning aerosol radiative and
379 climate effects on the Amazon rainforest prouctivity with an Earth system model.
380 *Atmos*. *Chem*. *Phys*., 19: 1301–1326. https://doi.org/10.5194/acp-19-1301-2019
381 Malhi, Y., Aragão, L. E., Galbraith, D., Huntingford, C., Fisher, R., Zelazowski, P., ... &
382 Meir, P. (2009). Exploring the likelihood and mechanism of a climate-change-
383 induced dieback of the Amazon rainforest. *Proceedings of the National Academy of*
384 *Sciences*, 106(49), 20610-20615. https://doi.org/10.1073/pnas.0804619106.
385 Morton, D. C., Nagol, J., Carabajal, C. C., Rosette, J., Palace, M., Cook, B. D., ... & North,
386 P. R. J. (2014). Amazon forests maintain consistent canopy structure and greenness
387 during the dry season. Nature, 506(7487), 221–224. https://dx.doi.org/10.1038/
388 nature13006.
389 Moura, Y. M., Galvão, L. S., Santos, J. R., Roberts, D. A., Breunig, F. M. (2012). Use of
390 MISR/Terra data to study intra- and inter-annual EVI variations in the dry season of
391 tropical forest. *Remote Sensing of Environment*, 127: 260–270.
392 https://doi.org/10.1016/j.rse.2012.09.013.
393 Moura, Y.M., Galvão, L.S., Hilker, T., Wu, J., Saleska, S., do Amaral, C.H., Nelson, B.W.,
394 Lopes, A.P., Wiedeman, K.K., Prohaska, N. and de Oliveira, R.C. (2017). Spectral
395 analysis of amazon canopy phenology during the dry season using a tower
396 hyperspectral camera and modis observations. *ISPRS journal of photogrammetry*
397 *and remote sensing*, (131):52-64. https://doi.org/10.1016/j.isprsjprs.2017.07.006

398 Murali, K. S., & Sukumar, R. (1993). Leaf flushing phenology and herbivory in a tropical
399 dry deciduous forest, southern India. *Oecologia*, 94(1), 114–119.993.
400 https://doi.org/10.1007/BF00317311.
401 Papaioannou, G., Papanikolaou, N., & Retalis, D. (1993). Relationships of
402 photosynthetically active radiation and shortwave irradiance. *Theoretical and*
403 *Applied Climatology*, 48(1), 23–27.
404 Phillips, O. L., Aragão, L. E., Lewis, S. L., Fisher, J. B., Lloyd, J., López-González, G., …
405 & Torres-Lezama, A. (2009). Drought sensitivity of the Amazon rainforest. *Science*,
406 323(5919), 1344–1347. https://doi.org/10.1126/science.1164033.
407 Rap, A., Spracklen, D.V., Mercado, L., Reddington, C.L., Haywood, J.M., Ellis, R.J.,
408 Phillips, O.L., Artaxo, P., Bonal, D., Restrepo Coupe, N., Butt, N., (2015). Fires
409 increase Amazon forest productivity through increases in diffuse radiation.
410 *Geophysical Research Letters*, 42(11): 4654-4662.
411 https://doi.org/10.1002/2015GL063719.
412 Roberts, D. A., Nelson, B. W., Adams, J. B., & Palmer, F. (1998). Spectral changes with
413 leaf aging in Amazon caatinga. *Trees*, 12(6), 315–325.
414 https://doi.org/10.1007/s004680050157.
415 Saleska, S. R., Didan, K., Huete, A. R., & da Rocha, H. R. (2007). Amazon forests green-
416 up during 2005 drought. *Science*, 318(5850), 612.
417 https://dx.doi.org/10.1126/science.1146663.
418 Samanta, A., Ganguly, S., & Myneni, R. B. (2011). MODIS enhanced vegetation index
419 data do not show greening of Amazon forests during the 2005 drought. *New*
420 *Phytologist*, 189(1), 11–15. https://dx.doi.org/10.1111/j.1469-8137.2010.03516.x.

421 Santos, V., Ferreira, M., Rodrigues, J., Garcia, M., Ceron, J., Nelson, B.W., Saleska,
422 S.R.(2018).Causes of reduced leaf-level photosynthesis during strong El Niño
423 drought in a Central Amazon forest. *Global Change Biology*, 24, 4266–4279.
424 https://doi:10.1111/gcb.14293.
425 Strada, S., & Unger, N. (2016). Potential sensitivity of photosynthesis and isoprene
426 emission to direct radiative effects of atmospheric aerosol pollution, *Atmos*. *Chem*.
427 *Phys*., 16: 4213–4234. https://doi.org/10.5194/acp-16-4213-2016.
428 Valle, D. F. (2016). *Seasonality of canopy leaf turnover is consistent along a toposequence*
429 *and maintains correlation with mean historical precipitation during a severe*
430 *drought year in a Central Amazon upland forest*, M.Sc Thesis, National Institute for
431 Amazon Research, 46 p. (in Portuguese). Retrieved from:
432 https://sucupira.capes.gov.br/sucupira/public/consultas/coleta/trabalhoConclusao/vie
433 wTrabalhoConclusao.jsf?popup=true&id_trabalho=3826868#
434 Wagner, F. H., Hérault, B., Rossi, V., Hilker, T., Maeda, E. E., Sanchez, A., ... Aragão, L.
435 E. (2017). Climate drivers of the Amazon forest greening. *PloS one*, 12(7),
436 e0180932. https://doi.org/10.1371/journal.pone.0180932.
437 Woebbecke, D. M., Meyer, G. E., Von Bargen, K., & Mortensen, D. A. (1995). Color
438 indices for weed identification under various soil, residue, and lighting conditions.
439 *Transactions of ASAE*, 38(1), 259–269.
440 Wu, J., Albert, L. P., Lopes, A. P., Restrepo-Coupe, N., Hayek, M., Wiedemann, K. T., ...
441 Saleska, S. R. (2016). Leaf development and demography explain photosynthetic
442 sea- sonality inAmazon evergreen forests. *Science*, 351(6276), 972–976.
443 https://dx.doi.org/ 10.1126/science.aad5068.

Wu, J., Kobayashi, H., Stark, S. C., Meng, R., Guan, K., Tran, N. N., ... Oliviera, R. C. (2018) . Biological processes dominate seasonality of remotely sensed canopy greenness in an Amazon evergreen forest. *New Phytologist*, 217(4),1507–1520. https://dx.doi.org/ 10.1111/nph.14939.

Xu, L., Samanta, A., Costa, M. H., Ganguly, S., Nemani, R. R., & Myneni, R. B. (2011). Widespread decline in greenness of Amazonian vegetation due to the 2010 drought. Geophysical Research Letters, 38(7). https://doi.org/10.1029/2011GL046824.

Yang, X., Tang, J., & Mustard, J. F. (2014). Beyond leaf color: Comparing camera-based phe- nologicalmetricswith leaf biochemical, biophysical and spectral properties through- out the growing season of a temperate deciduous forest. *Journal of Geophysical Research: Biogeosciences*, 119(3), 181–191. https://dx.doi.org/10.1002/ 2013JG002460.

8. List of Figure Captions

Fig 1. A) Long term monthly mean precipitation (black line) and monthly precipitation from May 2015 to Aug 2016 (red line) at ATTO tower site; B) Maximum cumulative water deficit (MCWD) shown for all sets of consecutive dry months from 1998 to 2016 at k34 and ATTO towers; C) Long term monthly means (black line) of daily maximum near-surface air temperature (^{o}C) and monthly values from May 2015 to Aug 2016 (red line) at ATTO tower; D) Long term monthly means (black line) and monthly values from May 2015 to Aug 2016 (red line) at ATTO, of surface shortwave downwelling radiant flux (watts m^{-2}), based on 24h mean flux under all-sky conditions. Long-term ± 1 SD envelopes are shown as black dashed lines in panels A, C & D. Grey shading indicates six consecutive months during the 2015/16 ENSO with precipitation below -1 SD (and below 100 mm mo^{-1}) at ATTO. Sources are TRMM 3B43v7, 1998-2018, for Panels A & B; MERRA-2 Reanalysis, 1980-2018, for panel C; CERES-EBAF Edition 4, 2000-2018, for panel D.

Fig 2. Post El Niño year 2016 (green) and the long-term monthly means ± 1SD for the fraction of all upper canopy crowns that massively produced new leaves at ATTO tower.

Fig. 3. (A) Standardized anomalies of MODIS-MAIAC Gcc for the 16 annual periods of Jun-Jul at ATTO tower (black bars) plotted against the percentage of recently flushed crowns in this same two-month period (green trace); Jun-Jul is when massively flushing crowns reach their annual peak under normal climate (see Fig. 2); (B) same as A, but for k34 tower. The “percentage of crowns”

476 that recently flushed is with respect to the total number of crowns that flushed in a year; non-
477 flushing crowns are excluded from the calculation.

478

479 **Fig 4**. A) Anomalies of MODIS-MAIAC EVI at the ATTO site for the second trimester of each
480 year (Apr-May-Jun) and the percentage of crowns with massively flushed leaves reaching early
481 mature stage (2-3 months age at ATTO and 2-4 months age at K34), also in the second trimester of
482 each year. The "percentage of crowns" is with respect to the total number of crowns that flushed in
483 a year; non-flushing crowns are excluded from the calculation.

484

Figure 1
Click here to download Figure: Figure_1.pdf

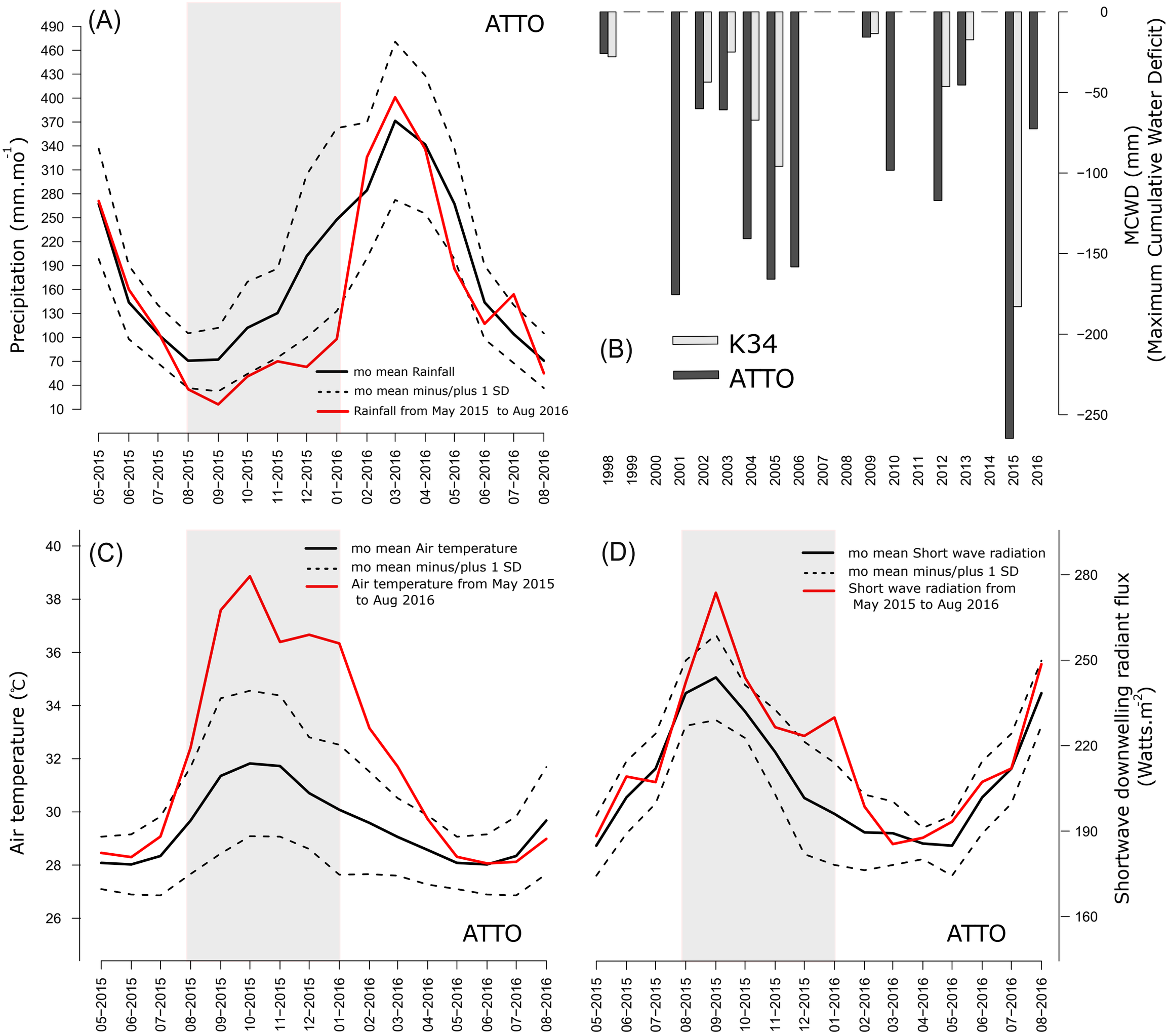

Figure 2

Click here to download Figure: Figure_2.pdf

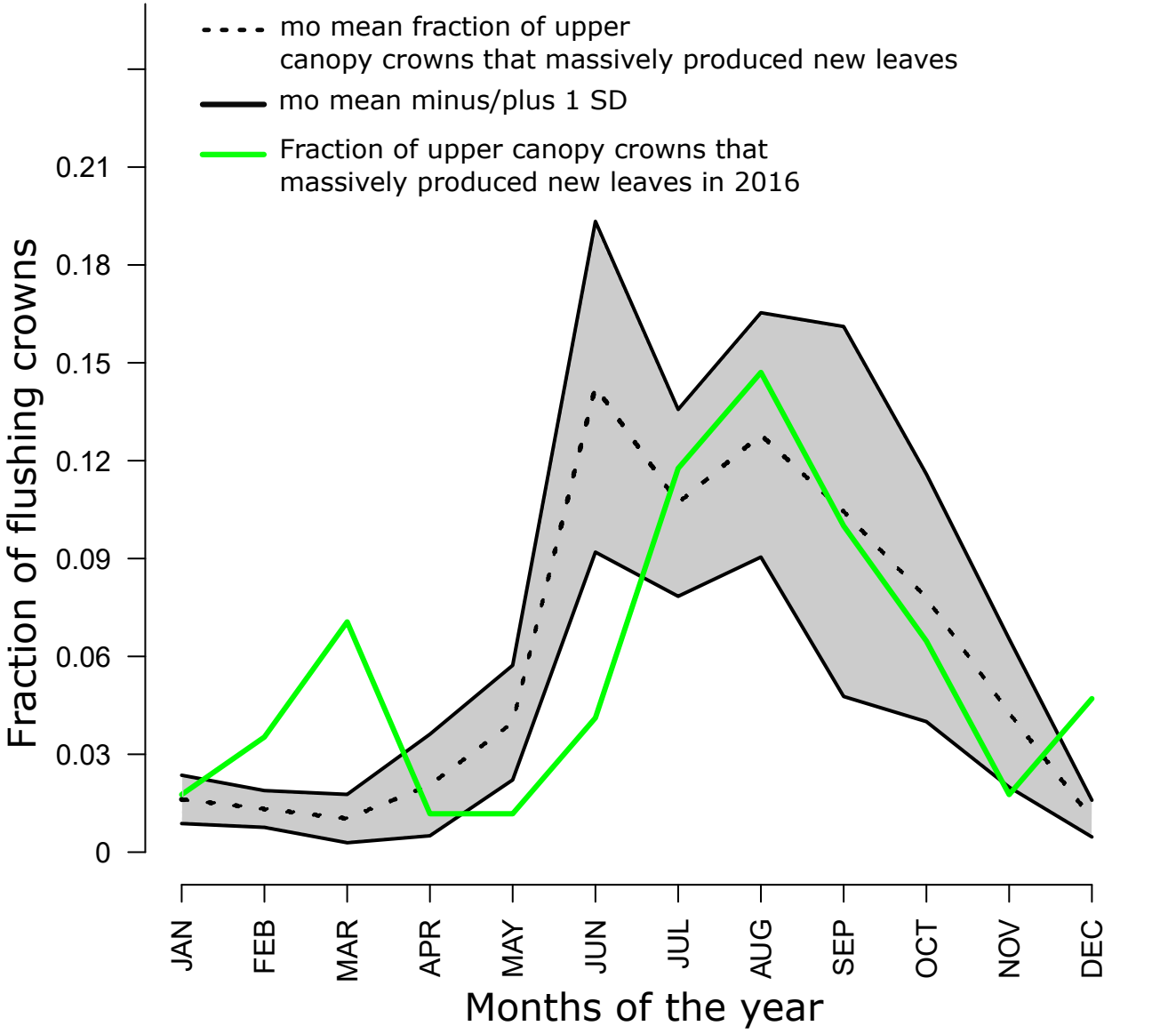

Figure 3
Click here to download Figure: Figure_3.pdf

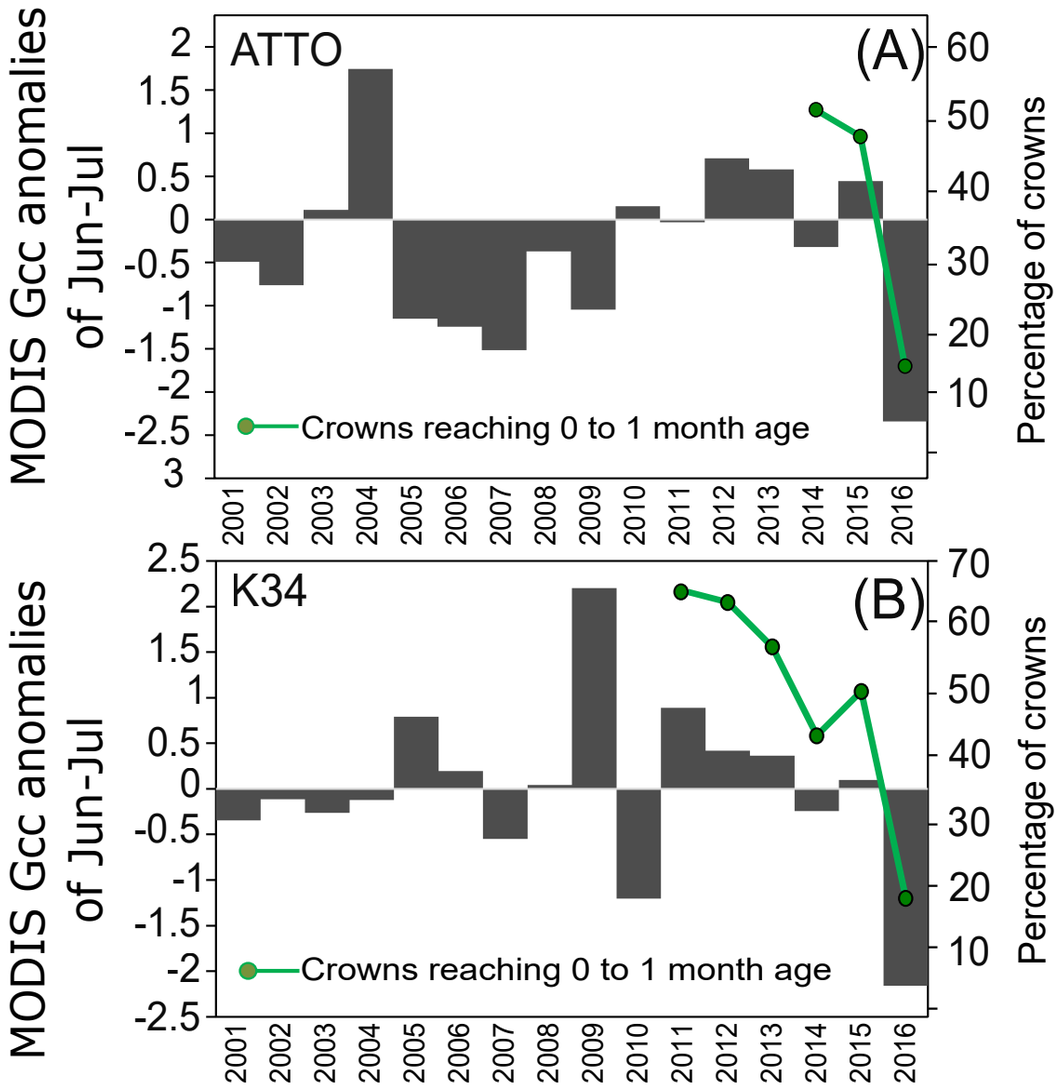

Figure 4

Click here to download Figure: Figure_4.pdf

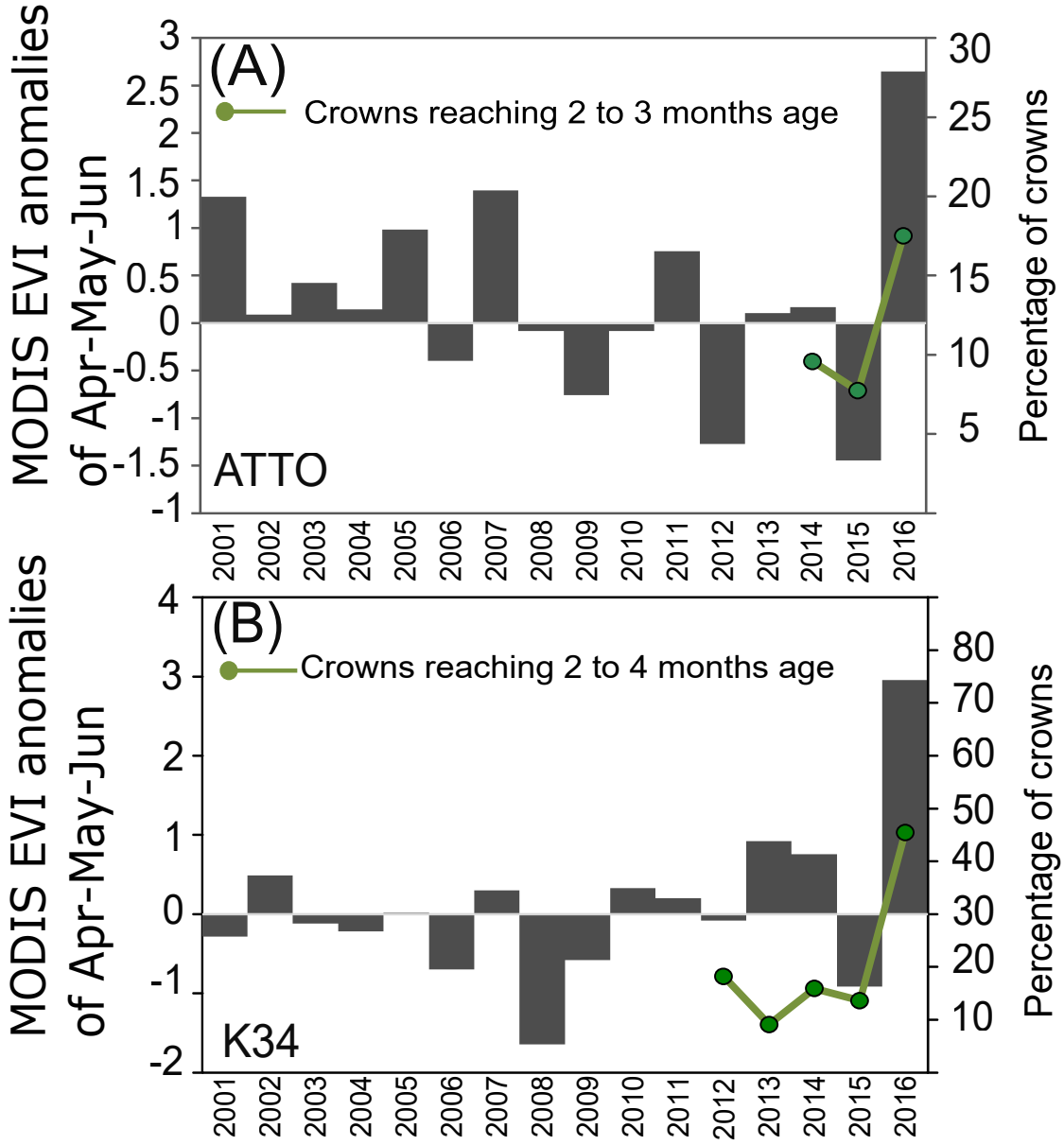

Supplementary Data 1

Click here to download Supplementary Data: Supp_Data1_Goncalves_etal_reviewed.docx

Supplementary Data 2

Click here to download Supplementary Data: Supp_Data2_Goncalves.pptx